Donor structure and electric transport mechanism in β-Ga_2O_3

Mitsuo Yamaga
Department of Mathematical and Design Engineering, Faculty of Engineering, Gifu University, Gifu 501-1193, Japan

Encarnación G. Víllora, Kiyoshi Shimamura, and Noboru Ichinose
Waseda University, 2-8-26, Nishiwaseda, Shinjuku, Tokyo 169-0051, Japan

Makoto Honda
Faculty of Science, Naruto University of Education, Naruto 772-8502, Japan

(Received 10 March 2003; revised manuscript received 28 July 2003; published 21 October 2003)

The electron paramagnetic resonance (EPR) study of β-Ga_2O_3 crystals gives evidence that donors can be regarded as O^{2-} vacancies trapping single electrons. The Lorentzian line shape of the EPR spectra observed in the range of 5–300 K, which exhibit anisotropic g values, suggests that motional narrowing occurs in this temperature range. For any magnetic-field orientation a single EPR line is observed, indicating that donor electrons are predominantly created in one of the three different oxygen sites in the β-Ga_2O_3 crystal. A previous transmission electron microscopy study suggested that a break of symmetry in domains of 2–3 nm correlates with a preceding cluster model of oxygen vacancies. From the temperature dependence of the EPR linewidth and the electrical conductivity it is found that the electron conduction in the clusters and/or between them is governed by a tunneling process at low temperatures, whereas at temperatures above 50 K, the transport of electrons through hopping between the clusters is thermally activated.

DOI: 10.1103/PhysRevB.68.155207 PACS number(s): 61.14.−x, 76.30.−v, 72.20.−i, 61.10.−i

I. INTRODUCTION

β-Ga_2O_3 belongs to the group of transparent conductive oxides (TCO) with a wide band gap and electrical conductivity. In the last decades, indium tin oxide (ITO) has been extensively investigated due to important applications such as flat panel displays, thermal windows, and solar cells.[1] Among the TCO's, β-Ga_2O_3 exhibits at present the largest band gap, $E_g = 4.8$ eV,[2] and thus a unique transparency from the visible into the UV region, where the cutoff wavelength is about 260 nm. β-Ga_2O_3 is, therefore, attracting much attention for the future generations of optoelectronic devices operating at shorter wavelengths,[3,4] where standard TCO's including ITO are already opaque.

The electrical conductivity of the TCO's is attributed to the existence of oxygen vacancies, which is caused by the tendency of all these oxides to deviate from the stoichiometric composition.[5] The amount of oxygen vacancies induced depends mainly on the growth atmosphere, and determines the electrical character of the specimens, which in the case of β-Ga_2O_3 can vary from insulating to conductive.[6,7] The other presumably identified common feature is that the TCO's form edge-shared octahedral (MO_6) chains.[8]

The defects in β-Ga_2O_3 are oxygen vacancies surrounded by cations. There are two notations to describe the type of defect and its effective charge relative to a normal lattice site, e.g., the Kröger-Vink (KV) notation[9] and the spectroscopic notation. In this paper, the KV notation for materials with the electrical conductivity induced by point defects is adopted. Oxygen vacancies compensated by two electrons or one electron, and not compensated are denoted as V_O^x, $V_O^\bullet$, and $V_O^{\bullet\bullet}$, respectively, where the subscript O indicates the oxygen site and the superscript indicates the net effective charge, neutral, $+1$, and $+2$.

β-Ga_2O_3 has oxygen ions in three different sites, denoted as O(1), O(2), and O(3) (the symmetry is depicted in Fig. 1).[10] Although, as stated by other authors (see below), electrons trapped at the oxygen vacancies are the origin of the electrical conductivity, the conduction mechanism is not yet fully understood. So, for example, which of the three oxygen sites is primarily related to the donor structure, and therefore linked to the electrical transport phenomenon, has not yet been experimentally determined.

Hajnal *et al.*[11] estimated by semiempirical quantum-chemical calculations that the formation energies of V_O^x located at O(1), O(2), and O(3) in β-Ga_2O_3 are 6.3, 5.3, and 4.0 eV, respectively, while the respective formation energies of $V_O^{\bullet\bullet}$ are 5.2, 4.3, and 6.1 eV. They did not calculate the formation energies of $V_O^\bullet$, which may be close to the average between those of V_O^x and $V_O^{\bullet\bullet}$. The top of the valence band corresponds to $2p$(O) states, and the bottom of the conduction band to $4s$(Ga) states. According to their calculation, the energy levels of V_O^x are located at 4.2, 4.3, and 2.8 eV above the top of the valence band. They also calculated the conduction-electron density as a function of the temperature and indicated a pure electronic character above 900 °C. They suggested that, under the assumption of a constant concentration of oxygen vacancies, the carrier density can be explained in terms of a thermal equilibrium between the two defects with the lowest formation energies, namely, $V_O^x(3)$ and $V_O^{\bullet\bullet}(2)$, where the numbers in parentheses indicate corresponding oxygen sites. Consequently, Hajnal *et al.* concluded that (i) $V_O^x(1)$ can be disregarded due to the relatively high formation energy, (ii) $V_O^x(3)$ leads to a deep donor level that cannot be ionized even at very high temperatures, and (iii) the carriers are provided through a thermal equilibrium between $V_O^x(3)$ and $V_O^{\bullet\bullet}(2)$.

Gourier's group[12,13] has reported that the conduction electrons exhibit a delocalized behavior in electron paramagnetic

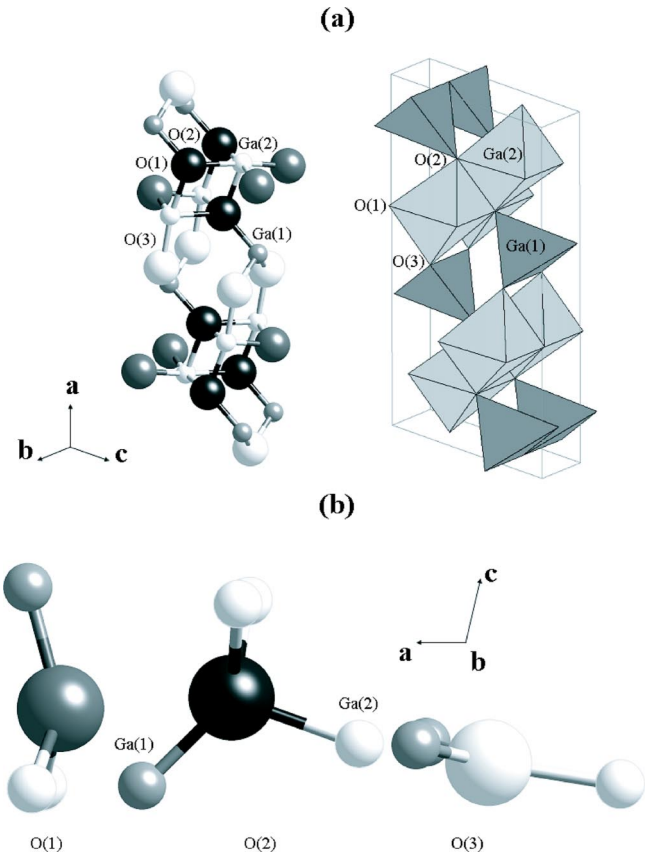

FIG. 1. (a) Three-dimensional crystal structure of β-Ga_2O_3 with a unit cell. Three oxygen sites with different symmetry are denoted by O(1), O(2), and O(3). Gallium atoms are in tetrahedral or octahedral coordination, denoted by Ga(1) and Ga(2), respectively. (b) Projection of the three oxygen complexes O(1), O(2), and O(3) along the *b* axis (slightly tilted).

resonance (EPR) measurements, that is, dynamic nuclear polarization by the Overhauser effect and narrow EPR lines are interpreted as motional narrowing. Although the small temperature dependence of the conductivity from room to liquid-helium temperatures further support the electron delocalization, the large Stokes shift in the blue luminescence indicates, on the contrary, electron localization. To accommodate both models, they have proposed that oxygen vacancies assemble, forming donor clusters that fulfill the Mott criterion for impurity band conduction, i.e., the oxygen vacancy concentration is large enough to achieve the overlap of the electron wave functions between adjacent clusters. The cluster size has been suggested to be about few nm from a transmission electron microscopy (TEM) study.[14] The donor-state energy levels are experimentally determined to be located at $E_d \sim 0.04$ eV below the bottom of the conduction band.[13] Thus, the paramagnetic centers are delocalized and exhibit a degenerate semiconductor behavior even when trapped in donor states at low temperatures.

In this paper, we propose donor structure and electric conduction mechanism in β-Ga_2O_3 single crystals. The study is carried out in terms of EPR, infrared (IR) absorption, electrical resistivity, single-crystal and powder x-ray-diffraction measurements.

II. EXPERIMENTAL PROCEDURE

Single crystals of pure and Sn-doped β-Ga_2O_3 were grown by the floating-zone technique. Feed rods were prepared by a sintering process, in which β-Ga_2O_3 powder of $4N$ purity and mixed powder of 97 mol % β-Ga_2O_3 and 3 mol % SnO_2 were pressed at room temperature and subsequently annealed under air at 1500 °C for 10 h. Crystals were grown with a pulling down rate of 5 mm/h and a constant gas flow rate of 500 ml/min. The growth atmosphere was oxidative in order to suppress the evaporation from the molten zone. Due to the decomposition of Ga_2O_3 into GaO and O_2 at the high growth temperatures, the compositions of as-grown crystals deviate from the stoichiometric, as in general for TCO's. Annealing for six days at 900 °C under a 1 atm O_2 atmosphere was carried out for the pure as-grown crystals. The pure as-grown crystals were electrically conductive, with a carrier density of about $10^{17}-10^{18}$ cm^{-3}, whereas the annealed crystals became insulating, in accordance with a previous report.[15] Samples were prepared by cleaving along the (100) and (001) planes, with approximate dimensions of $0.2-0.5\times7\times7$ mm^3 for optical and electrical resistivity measurements, and $\sim0.2\times2\times0.5$ mm^3 for EPR and single-crystal x-ray-diffraction measurements.

Single-crystal x-ray diffraction was performed with a Mac Science MXC 4-cycle diffractometer at room temperature, while powder x-ray diffraction was measured from liquid-helium temperature up to 1000 °C using a Rigaku Rint-TTR diffractometer. Above room temperature a Pt holder was utilized, while a Cu one below. In both x-ray experiments, the $Cu_{\alpha 1}$ emission line was utilized as radiation source. Single-crystal diffraction enables the accurate measurement of defined single reflections, after the crystal orientation has been determined. The lattice parameters were estimated by the Rietveld analysis.

Constituent elementary analyses were performed with a Shimadzu ESCA-850 equipment.

EPR measurements were carried out using a JES-FA200 *X*-band spectrometer with microwave frequencies of $\sim$9.206–9.209 GHz at 293 K. Low-temperature EPR spectra were measured using a Bruker EMX10/12 *X*-band spectrometer with $\sim$9.62–9.69 GHz in the range of 5–300 K. Both spectrometers employed 100 kHz field modulation.

Optical absorption spectra were measured at 293 K using a Hitachi U-3500 spectrometer in the range of 180–3000 nm.

Electrical resistivity measurements in the temperature range of 5–300 K were done using an Accent HL5500PC Hall-effect measurement equipment without magnetic field. Ohmic electrodes realized by Au sputtering on the (100) plane were located on the edge of the specimen in a quadrangle configuration, which conforms to the van der Pauw method. The specimens were measured under dark conditions, in order to avoid the photogeneration of free carriers.

III. CRYSTAL STRUCTURE

β-Ga_2O_3 has monoclinic structure, with the space group $C2/m$.[10] The lattice parameters at room temperature are measured to be $a=12.23$ Å, $b=3.040$ Å, $c=5.807$ Å and the

TABLE I. Atomic positions of β-Ga_2O_3.

Atom	x	z	Coordination
Ga(1)	0.0904	0.7948	fourfold
Ga(2)	0.3414	0.6857	sixfold
O(1)	0.1674	0.1011	threefold
O(2)	0.8279	0.4365	fourfold
O(3)	0.4957	0.2553	threefold

unique axis $\beta = 103.7°$. Figure 1(a) shows the unit cell, which contains four formula units. Eight Ga atoms and twelve O atoms are evenly distributed into two Ga and three O nonequivalent sites at positions $4i$, (0,0,0;1/2,1/2,0) $(x,0,z)$ (Table I).[16,17] Ga ions are surrounded by O ions in either tetrahedral, Ga(1), or octahedral coordination, Ga(2), while one oxygen site is in tetrahedral coordination and the other two sites are threefold coordinated. The three oxygen sites are denoted as O(1), O(2), and O(3). Figure 1(a) also illustrates how O(1) and O(3) are located at the edge shared by a Ga(1) and a Ga(2) chain, whereas O(2) is at the edge shared by a Ga(1) and two Ga(2) chains.

Figure 1(b) shows the projection of the three oxygen complexes along the *b* axis. The structure is as follows: O(1), bond not in plane to two Ga(2) and one Ga(1) ions; O(2), bond in tetrahedral coordination with three Ga(2) and one Ga(1); O(3): bond in plane to two Ga(1) and one Ga(2) ions.

β-Ga_2O_3 presents two cleavage planes, the main one is the (100) plane, and the secondary the (001). The first correlates with the O(3) site, while the second with the O(1) and O(2) sites, indicating clearly the order of bonding strength, that varies from O(2), O(1) to O(3), also from higher to lower coordination.

IV. EXPERIMENTAL RESULTS

A. X-ray and electron diffraction

According to the space-group and sites symmetry, the observable reflections in the case of β-Ga_2O_3 are defined by the general selection rules:[17] (hkl), $h+k=2n$; $(h0l)$, $h=2n$; $(0kl)$, $k=2n$; $(hk0)$, $h+k=2n$; $(0k0)$, $k=2n$; $(h00)$, $h=2n$; with n integer (1,2,3,4,5). Single-crystal diffraction measurements indicated that the pure as-grown samples as well as the annealed ones fulfill these selection rules.

In Table II are listed the measured integrated intensities of representative directions normalized by the (020) reflection, which showed a maximum intensity for the as-grown sample among the regarded reflections. After annealing, the intensity of the (020) reflection diminished by about 15%, contrasting with the about 60% increase of the (002) reflection, which became the most intense. Therefore, Table II indicates that annealing promotes a remarkable increase of the (002) and (004) reflections, while no remarkable variation is observed for the $(h00)$ reflections.

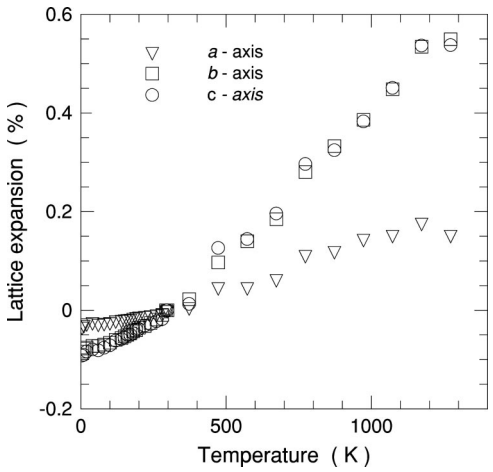

FIG. 2. Temperature dependence of the lattice parameters in the range 4–1273 K for the pure as-grown β-Ga_2O_3 crystal. The lattice expansion (Δl) is expressed relative to those measured at room temperature, according to $\Delta l = [l(T) - l(293)]/l(293)$ where $l(T)$ denotes each of the *a*, *b*, and *c* lattice parameters at the temperature *T*.

The presence of oxygen vacancies produces inward and outward displacements of ions, resulting in reduction of symmetry. Then, allowed reflections might reduce in intensity and forbidden reflections might be detectable. The results in Table II suggest that annealing does not remarkably affect the oxygen concentration in the O(3) site, clearly linked to the (100) plane, instead promotes a notable decrease in the concentration of vacancies on the sites O(1) and/or O(2), which are contained in the planes parallel to the (001) plane.

Figure 2 shows the temperature dependence of the lattice parameters, expressed relative to the values measured at 293 K for the pure as-grown β-Ga_2O_3 crystals ($a = 12.23$ Å, $b = 3.040$ Å, and $c = 5.807$ Å), in the range of 4–1273 K. The lattice expansion coefficient (4.2×10^{-6} K^{-1}) along the *b* and *c* axes is three times larger than that (1.4×10^{-6} K^{-1}) along the *a* axis, indicating that the lattice expansion takes place principally in the (100) plane.

TABLE II. Single-crystal x-ray integrated reflection intensities for the pure as-grown and annealed β-Ga_2O_3 crystals. Measured values are given relative to the (020) reflection (100 %). $(h00)$ with $h \geq 12$, $(0k0)$ with $k \geq 4$, and $(00l)$ with $l \geq 5$ are over the available goniometer range.

h	0	2	4	6	8	10	0	0	0	0
k	2	0	0	0	0	0	0	0	0	0
l	0	0	0	0	0	0	1	2	3	4
As-gr.(%)	100	<0.05	91.0	41.2	11.3	0.6	13.1	70.7	0.2	8.1
Ann.(%)	100	<0.05	98.2	41.5	9.5	<0.05	15.8	134.4	0.3	13.8

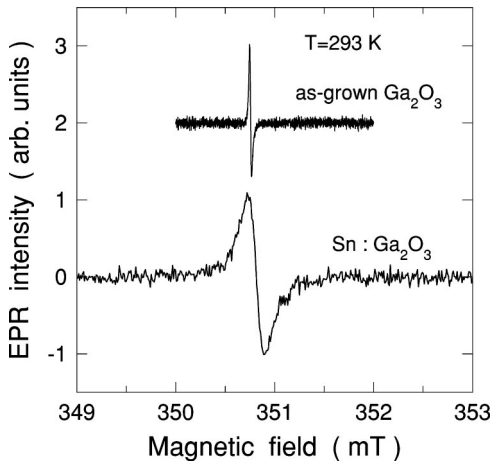

FIG. 3. EPR spectra for the pure and Sn-doped as-grown β-Ga_2O_3 crystals with the magnetic field applied perpendicular to the (100) plane at 293 K.

The results obtained by electron-diffraction experiments have been described in detail in a previous paper.[14] The TEM observations indicated that there is a local break of symmetry in small domains of average size below 5 nm. The forbidden $(10\bar{2})$ reflection was found at the 1/2 position between the main reflections along the $q_{(20\bar{4})}$ vector. The plane distance corresponding to the diffuse scattering at the 1/2 position is 2.90 Å, i.e., half the *c* lattice constant. The 1/2 position intensity weakened after annealing in an O_2 atmosphere. Since the annealed sample had changed from conductive to insulating, it was suggested that the diffuse scattering is related with the existence of oxygen vacancies, whose concentration in small domains can be linked with the donor-cluster model proposed by Binet *et al.*[13]

The electron spectrocopy for chemical analysis elementary analyses of pure and Sn-doped samples were done using integrated intensities of the lines at the characteristic energies, 532 eV and 21.4 eV, of O(1*s*) and Ga(3*d*), respectively. The elementary ratios of Ga to O for the pure as-grown and annealed samples were obtained to be 43:57 with the experimental errors of ±2%. Although the as-grown sample was expected to have large deviation from stoichiometry in comparison with that of the annealed sample, there was no difference in the ratios. In addition, the Sn signals from the Sn-doped sample could not be detected. The Sn concentration of the nominally 3 mol % SnO_2 doped sample may be less than the experimental precision of 2–3 at %.

The direct evidence for the oxygen vacancies could not be obtained by the above x-ray and electron diffraction, and chemical analysis. In order to elucidate the structure of the donor cluster, further experiments and more complex analyzing techniques are required.

B. EPR

Figure 3 shows the EPR spectra observed for the pure and Sn-doped as-grown β-Ga_2O_3 crystals with the magnetic field applied perpendicular to the (100) plane at 293 K with a microwave power of 0.1 mW and a frequency of ~9.618 GHz. Each EPR spectrum consists of a single sharp line at 350.8 mT. Sn doping leads to an increase of the linewidth by about one order of magnitude, instead, annealing decreases the intensity by about two orders of magnitude (not shown).[18]

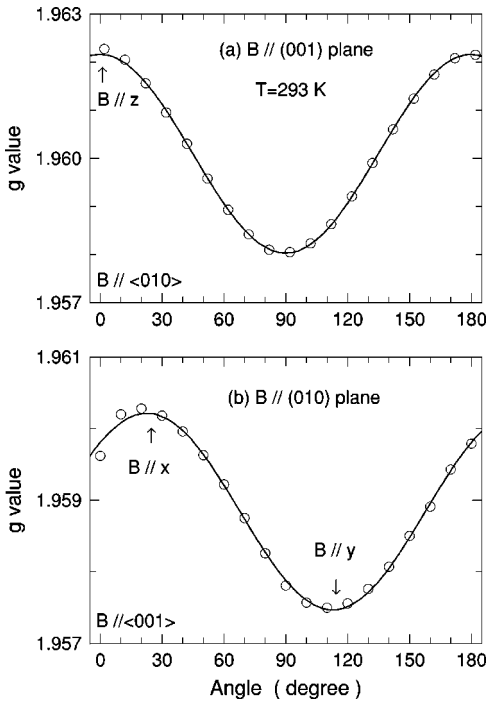

FIG. 4. Angular variations of the EPR lines for the pure as-grown β-Ga_2O_3 crystal measured at 293 K in (a) the (001) plane and (b) the (010) plane. The solid curves are calculated using Eq. (1) with the parameters $(g_x, g_y, g_z)=(1.960,1.958,1.962)$.

Figure 4 shows the angular variations of the EPR lines in the (001) and (010) planes for the pure as-grown sample at 293 K. The angular dependence can be described by a spin Hamiltonian with orthorhombic symmetry in the form of[19]

$$\mathcal{H}=\mu_B g_x B_x S_x+\mu_B g_y B_y S_y+\mu_B g_z B_z S_z, \qquad (1)$$

where μ_B is the Bohr magneton, *B* is a resonance magnetic field, and $S(=\frac{1}{2})$ is an effective spin. The *g* value of the *z* axis is determined experimentally to be substantially different from the two other *g* values. The principal *z* axis of orthorhombic centers is parallel to the crystalline *b* axis. The *x* and *y* axes are rotated around the *b* axis by θ and $\theta+\pi/2$ angles from the *c* axis, respectively. The solid curves in Fig. 4, calculated using Eq. (1) with the *g* values of $(g_x, g_y, g_z)=(1.960,1.958,1.962)$ and an angle of $\theta=24°$ for the pure as-grown sample are in good agreement with the experimental points. The *g* values of the Sn-doped and annealed samples observed at 293 K are the same as those of the pure as-grown sample within experimental errors.

The ground state of V_O^x in oxides is a spin-singlet state, being insensitive to EPR. Instead, $V_O^{\bullet}$ consisting of an unpaired electron are paramagnetic. The EPR lines with the negative *g*-shift from the *g* value ($g_e=2.0023$) of the free electron are consequently assigned to $V_O^{\bullet}$ with $S=\frac{1}{2}$.

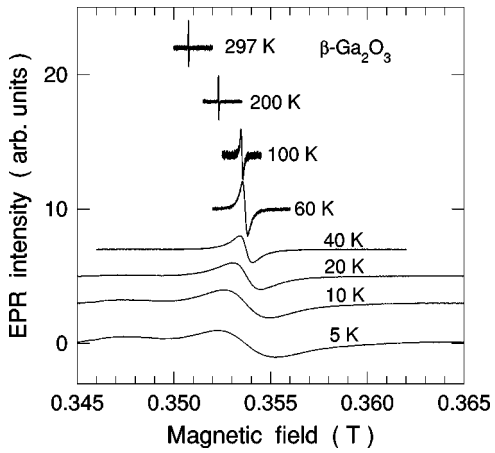

FIG. 5. Temperature dependence of the EPR spectra with the magnetic field applied perpendicular to the (100) plane for the pure as-grown β-Ga_2O_3 crystal.

The EPR spectra measured at different temperatures are shown in Fig. 5. The magnetic field was applied perpendicular to the (100) plane, the incident microwave power being about 1–50 μW in order to avoid saturation of the EPR signal. The resonance field in Fig. 5 shifted to higher fields when the temperature decreased. This corresponds to the shift of the cavity resonances to higher frequencies. In consequence, the observed g values are constant in the temperature range of 5–300 K within the experimental errors ($\pm$0.0007). A steep increase in the EPR linewidth in Fig. 5 was observed when the temperature was lowered below 100 K. This result is opposite to that found for paramagnetic centers in ionic crystals, where line broadening occurs by an enlarged lattice-spin relaxation rate at higher temperatures.[19]

Figure 6 shows the inverse of the linewidth ($1/\Delta B$) as a function of the inverse of the temperature ($1/T$) for the pure and Sn-doped as-grown samples. The temperature dependence of the linewidths for the Sn-doped as-grown sample differs from that for the pure as-grown sample. That of the annealed sample could not be observed because of the weak signals.

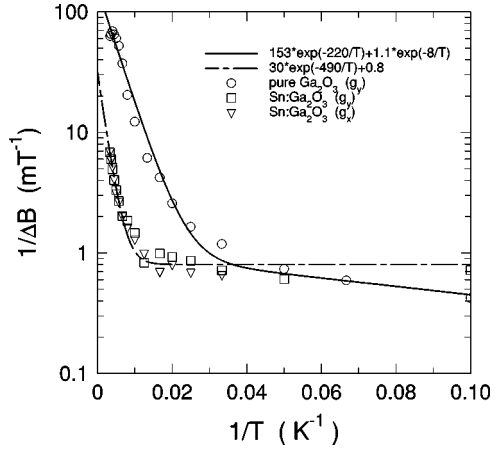

FIG. 6. Inverse of the linewidth ($1/\Delta B$) as a function of the inverse of the temperature ($1/T$) for the pure as-grown and Sn-doped β-Ga_2O_3 crystals. The solid and dashed curves calculated using exponential functions fit the experimental points very well.

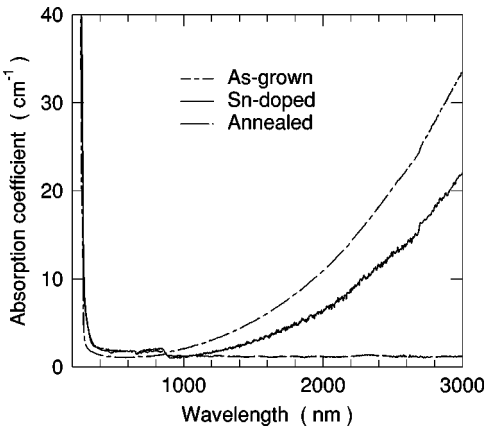

FIG. 7. Optical absorption spectra measured at 293 K for the pure as-grown, annealed, and Sn-doped β-Ga_2O_3 crystals.

C. Infrared absorption

Figure 7 shows the optical absorption spectra measured at 293 K in the range of 200–3000 nm for the pure as-grown, annealed, and Sn-doped β-Ga_2O_3 crystals. The band edges are observed approximately at 260 nm for all three samples.

The absorption coefficient for the pure as-grown sample as well as the Sn-doped sample gradually increases in the infrared wavelength region, 1000–3000 nm, whereas it is negligibly small for the annealed sample. The IR absorption is associated with the plasma frequency, which is determined by the free carrier density n (electrons/cm^3). A decrease in the carrier density leads to a shift of the plasma frequency to lower energies, that is, longer wavelengths. Concerning the pure as-grown samples, the carrier density was estimated to be $n \sim 10^{17}$–10^{18} (1/cm^3) by electrical measurements.[15] The associated plasma frequencies correspond to free space wavelengths in the order of $\sim$10–30 μm. On the other hand, although the annealed sample was electrically insulating, the EPR measurements suggested that the carrier density associated with $V_O^{\bullet}$ had diminished by only about two orders of magnitude.[18] The lack of plasma absorption for the annealed sample may be due to the shift of the plasma frequency to the very far IR, which is linked to the decrease in the carrier concentration as explained above. The annealing process promotes replacing $V_O^{\bullet\bullet}$ with O^{2-} and/or removing electrons from V_O^{x} and $V_O^{\bullet}$.

D. Electrical resistivity

The resistivity for the pure as-grown β-Ga_2O_3 crystal was measured by the van der Pauw method, which is based on the assumption of an isotropic electrical conduction. The measured values represent an average of the anisotropic ones along the c and b axis, which according to Ueda *et al.*[3] differ from each other by about one order of magnitude.

Figure 8 shows the temperature dependence of the inverse of the electrical resistivity, i.e., the conductivity, for the pure as-grown β-Ga_2O_3 crystal. Similar to the temperature dependence of the inverse linewidth of the EPR spectra, the conductivity exhibits in a first approximation an exponential dependence on the inverse temperature in the range

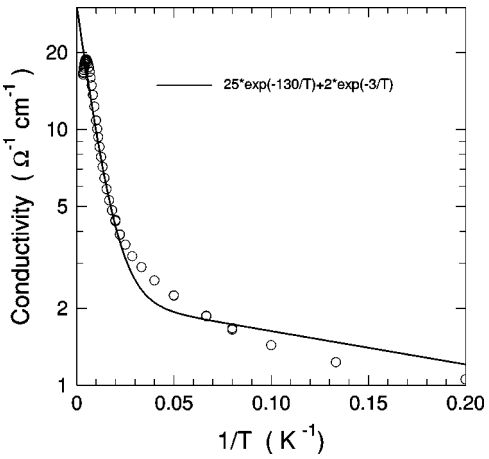

FIG. 8. Temperature dependence of the inverse of the electrical resistivity, i.e., the conductivity, for the pure as-grown β-Ga_2O_3 crystal.

from 40 up to about 120 K. The conductivity saturates above 120 K, reaches a maximum, and then decreases above 200 K. The decrease is probably related to phonon scattering of electrons.

V. DISCUSSION

A. EPR

Hajnal *et al.*[11] concluded from their calculations that the carrier density is determined by the thermal equilibrium between the concentrations of V_O^x and $V_O^{\bullet\bullet}$. In the calculations, however, the possibility for the formation of $V_O^{\bullet}$ was not taken into account. The EPR technique is a powerful tool to reveal localized and delocalized states of unpaired electrons. Although information on V_O^x cannot be obtained by EPR, it will be shown below, how from the results on $V_O^{\bullet}$ (namely, the line shapes, the temperature dependence of the linewidths, and the anisotropic g values) a model for the donor structure and the electron conduction mechanism can be worked out.

First, the line shape of the EPR spectrum is considered. As discussed by the Gourier's group,[12,13] the line broadening at low temperature is probably caused by a superhyperfine (shf) interaction between the electron spin and nuclear spins of near Ga ions in the form of[12]

$$\mathcal{H}_{shf}=\sum_{i=1}^{n} A_x^i I_x^i S_x + A_y^i I_y^i S_y + A_z^i I_z^i S_z, \tag{2}$$

where I^i is the nuclear spin of the ith Ga ligand ion and $A_j^i (j=x,y,z)$ is a shf coupling constant. The ^{69}Ga and ^{71}Ga isotopes with the natural abundance of 0.602 and 0.398, respectively, possess the nuclear spin of 3/2, and the magnetic moments of 2.01 and 2.55 respectively, in the unit of the nuclear magneton. Due to the s character of the conduction electron, the associated shf coupling constant is assumed to be isotropic, i.e., $A_j^i=A^i(j=x,y,z)$. When distances to Ga ions increase, the coupling constant of A^i decreases. As a consequence, the EPR spectrum is inhomogeneously broadened by the unresolved shf interaction and approximately represented by a Gaussian function.

Van Vleck[20,21] calculated how the line shape of a pair of the hyperfine line changes with the ratio of the exchange frequency to the hyperfine interaction frequency as parameter. The phenomenon is known as exchange narrowing. The line shape approximates to a Lorentzian for the strong exchange.

The fairly narrow EPR spectra at high temperatures, which are caused by motional narrowing,[12] are discussed in the same way as exchange narrowing predicted by Van Vleck.[20,21] The Lorentzian line shape is given in the form of

$$I(\omega)=\frac{I_0}{(\omega-\omega_0)^2+(\omega_{shf}^2/\omega_{mn})^2}, \tag{3}$$

where ω_0 is a resonance frequency, ω_{shf} is associated with a width of the resonance absorption induced by the shf interaction, and ω_{mn} represents that spin flips of electrons occur after $2\pi/\omega_{mn}$ through motional narrowing.

Localization or delocalization of electrons around the oxygen vacancies strongly corresponds to whether the observed EPR spectrum is represented by a Gaussian or Lorentzian line shape, respectively. Figure 9 shows the integration of the observed derivative curves together with the fitting curves for the pure and Sn-doped samples. In the case of the pure sample, the observed line shapes above 10 K fit Lorentzians except at 200 K with slight asymmetry. Below 10 K, the observed line shapes are intermediate between Lorentzian and Gaussian curves. Such behavior distinctly appears in the Sn-doped sample. There are three temperature regions: the line shape below 80 K fits a Gaussian, that above 130 K fits a Lorentzian, and that between 100–125 K is intermediate. These results suggest that (1) the donor electrons in the pure sample are delocalized even at 5 K and (2) those in the Sn-doped sample may be localized around the oxygen vacancies below about 80 K.

Next, let us consider the temperature dependence of the linewidth for the pure and Sn-doped samples in Fig. 6. The values of $\Delta\omega(=\omega_{shf}^2/\omega_{mn})$ in Eq. (3) can be obtained from the observed linewidth ΔB of the resonance in the unit of magnetic field. They satisfy the relation $\hbar\Delta\omega=g\beta\Delta B$, and thus ω_{mn} turns out to be inversely proportional to ΔB. The relation of $1/\Delta B$ versus $1/T$ for the pure and Sn-doped samples is shown in Fig. 6. The experimental data can be fitted by exponential functions, $153e^{-220/T}+1.1e^{-8/T}$ and $30e^{-490/T}+0.8$, respectively. The difference in the activation energy, 19 and 42 meV for the pure and Sn-doped samples, respectively, might be originated by a decrease in the concentration of $V_O^{\bullet}$ after Sn doping, since Fig. 7 indicates a decrease in plasma absorption for the Sn-doped sample relative to the pure one. Their behaviors $1/\Delta B$ at the higher-temperature range are consistent with a model for a thermally activated polaron hopping between $V_O^{\bullet}$'s.[22] The fairly small activation energy of 0.7 meV in the temperature range of 5–30 K for the pure sample suggests tunneling between $V_O^{\bullet}$'s rather than hopping. On the other hand, the values of $1/\Delta B$ for the Sn-doped sample is independent of the tem-

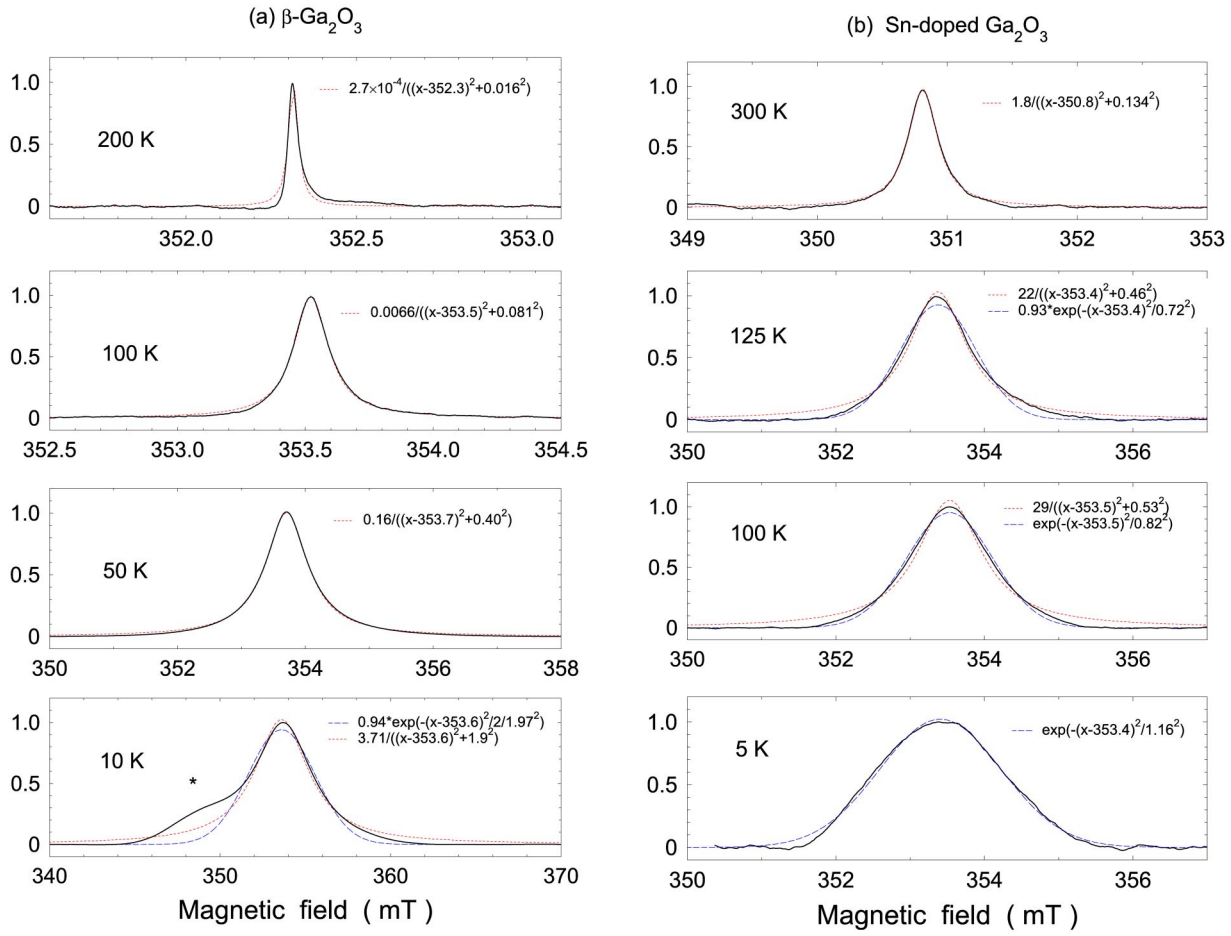

FIG. 9. (Color online) Integration of the observed derivative EPR spectra in the temperature range of 5–300 K for (a) pure as-grown sample and (b) Sn-doped sample with fitting Gaussian curves or Lorentzian curves. * in (a) denotes an impurity signal.

perature in the range of 5–100 K, suggesting the possibility that electrons are localized around $V_O^{\bullet}$ or transfer to near $V_O^{\bullet}$ through tunneling as well as the pure sample.

Motional narrowing observed in the EPR spectra at high temperatures is related to electron transfer, whose rate may be larger than the shf interaction frequency. Electrons are expected to transfer through hopping or tunneling between $V_O^{\bullet}$'s or through narrow impuritylike band conduction. Here, we consider the relation between the electron transfer and the anisotropic g tensor observed for the pure and Sn-doped samples when motional narrowing occurs.

If oxygen vacancies are created at the three O(1), O(2), and O(3) sites with equal probabilities, electrons are localized or delocalized around the oxygen vacancy sites with different symmetry as shown in Fig. 1(b). Electrons move at random between these three sites when temperature increases up to 300 K. As a consequence, the averaging between the EPR spectra with different configurations leads to an isotropic g tensor. However, the observed g tensors are anisotropic. This discrepancy may be removed by an assumption that motional narrowing occurs preferentially between ones of O(1), O(2), and O(3).

Which of the sites O(1), O(2), and O(3) is responsible for electron transfer is discussed in terms of the anisotropic g tensor. The principal axes of the g tensor are strongly associated with the structure of the oxygen complexes, shown in Fig. 1(b) and described as follows.

(i) The O(1) complex is composed of a Ga(1) and two Ga(2) ligands in a plane, except that Ga(1) is slightly bent from the c axis. One of the principal axes is parallel to the b axis, and the other is approximately parallel to the a axis. The remaining is perpendicular to the two defined axes.

(ii) The O(2) complex forms a tetrahedron consisting of a Ga(1) and three Ga(2) ligands. One of the principal axes is the direction along the combination of O(2) and Ga(1), which is rotated about 30° from the c axis. The other is parallel to the b axis. The remaining is perpendicular to the two defined axes.

(iii) The O(3) complex is composed of two Ga(1) and a Ga(2) ligands in a plane. The three principal axes are expected to be the c axis perpendicular to the plane, the b axis parallel to the direction combining the two Ga(1), and the direction combining O(3) and Ga(2).

The observed angular variations of the EPR lines in the (010) and (001) planes (Fig. 4) determine the principal axes. The principal z axis coincides with the crystalline b axis. The other two lie consequently in the (010) plane, the x axis being rotated 24° from the c axis to the a axis. This is consistent with the estimated structure of the O(2) complex, and indicates that $V_O^{\bullet}$'s are presumably generated in the O(2)

sites. From the above model, donor electrons in $V_O^{\bullet}(2)$ are expected to transfer along the *b* axis through hopping and tunneling because the O(2) sites are located at the edges sharing chains of octahedra and tetrahedra along the *b* axis [as shown in Fig. 1(a)].

Finally we consider formation of a narrow impuritylike band of donor electrons. Hajnal *et al.*[11] concluded that the conduction band-edge state can be extended states of one-dimensional chain of Ga atoms in the *b* lattice direction. Their calculation is consistent with the anisotropy of optical absorption edge in the range of 260–280 nm (Ref. 23) and the conductivity.[3,23] Recently, the peculiar peak structure in the optical absorption edge at low temperature was reported.[24] The peaks have been interpreted as transitions from discrete energy levels in low dimensional acceptor cluster with size about 3–4 nm. This acceptor cluster model is consistent with the result that the properties of the absorption edge could be observed even in the annealed sample. The blue luminescence broadband with a peak around 370 nm and the excitation bands with two peaks at 260 and 276 nm were observed in the pure as-grown sample, while these bands completely disappeared in the annealed sample.[18] These results suggest that (1) the excitation bands of the blue luminescence are due to transitions from the valence band to the donor levels, which are associated with the oxygen vacancies, and (2) the donor and acceptor absorption bands overlap in the range of 260–280 nm. As a consequence, the impuritylike donor band does not lie in the conduction-band edge, but below it.

The anisotropy of the donor band is not necessarily the same as that of the conduction band, with an assumption that the oxygen vacancies were created at random in the crystal. However, the preferential vacancy creation, which is similar to the one-dimensional chain of Ga atoms could induce the anisotropy. Further donor band calculation in the base of the preferential vacancy sites will be required.

B. Mechanism of the conductivity

Ueda *et al.*[3,23] reported strong anisotropy of the electrical properties for β-Ga_2O_3, the conductivity along the *b* axis being about one order of magnitude larger than that along the *c* axis. In the preceding section, we have concluded that vacancies are created preferentially at the O(2) sites, and that electrons in $V_O^{\bullet}$ move along the b axis. In this section, the relation between the crystal structure and the reported electric anisotropy is considered more in detail.

There are four O(2) alignments along the *b* axis in a unit cell as shown in Fig. 1(a). If oxygen vacancies are assumed to be created in the O(2) alignments, the shortest distance (2.6 Å) between two O(2) vacancies is along a direction tilted about 45° from the $\langle 101 \rangle$ to the *b* axis. The distances between two O(2) vacancies from further alignments are 3.0, 5.8, and 4.1 Å along the *b*, *c*, and *a* axis, corresponding to the *b* and *c* lattice parameters and one third of the *a* lattice parameter, respectively. The anisotropy of the conductivity along the *b* and *c* axes may be explained by the difference in the electron wave-function overlap between adjacent donors. The smaller distance between the O(2) sites along the *b* axis leads to the larger overlap, giving rise to the larger conductivity along this axis. However, as the cluster size found in the same samples by TEM (Ref. 14) are ~3 nm, the significant difference in the *b* and *c* lattice parameters is not enough to explain the anisotropy of the conductivity.

The temperature dependence of the conductivity for the pure sample in Fig. 8 can be represented by a double exponential function $25e^{-130/T}+2e^{-3/T}$, which is very similar to that of the inverse linewidth for the same sample in Fig. 6 except for half the activation energy. Both the inverse linewidth and the conductivity are almost constant below 50 K, but rapidly increase above 50 K. The following points are concluded.

(i) At low temperatures (below 50 K) the donor electrons tunnel between $V_O^{\bullet}$'s. The tunneling model is equivalent to the overlap of the electron wave functions in the donor states, i.e., the Mott criterion.

(ii) At high temperatures (above 50 K), the temperature behavior obeys the Arrhenius equation, being strongly associated with the thermal activation of polaron hopping.[22]

The TEM study indicates that the size of the donor clusters is ~3 nm.[14] Binet and Gourier[13,24] proposed that the conduction occurs by the electron hopping between donor clusters and that some of acceptors are assembled in low dimensional cluster with size about 3–4 nm. This charge transfer requires an activation energy, which increases as the distance between donors increases, i.e., as the concentration of $V_O^{\bullet}$ decreases. In agreement with this expectation, the activation energy for the Sn-doped sample is larger than that of the pure as-grown one (Fig. 6), since according to the plasma absorption in the IR (Fig. 7), the carrier concentration decreases after Sn doping.

VI. CONCLUSIONS

The electrical conductivity of the β-Ga_2O_3 crystals exhibits a semiconductor behavior even at very low temperatures. The carrier electrons, whose concentration correlates with that of oxygen vacancies, exhibit a delocalized behavior even when trapped at the oxygen vacancies. This observation is consistent with motional narrowing of the EPR spectra in the temperature range of 5–300 K, which show a Lorentzian line shape. Both the temperature dependence of the inverse linewidth and the conductivity can be described by the Arrhenius equation, where each curve includes exponential and constant terms. The exponential term suggests the transfer of electrons between the donor clusters by a thermally activated hopping process, whereas the constant term suggests a tunneling process in the clusters and/or between them.

ACKNOWLEDGMENTS

The authors would like to thank to M. Fujiwara of Kagami Memorial Laboratory for Materials Science and Technology, Waseda University, and T. Gotoh of Material Characterization Central Laboratory, Waseda University, for their continuous support in the crystal characterization.

[1] B.G. Lewis and D.C. Paine, MRS Bull. **25**, 22 (2000).
[2] H.H. Tippins, Phys. Rev. A **316**, 140 (1965).
[3] N. Ueda, H. Hosono, R. Waseda, and H. Kawazoe, Appl. Phys. Lett. **70**, 3561 (1997).
[4] M. Orita, H. Ohta, M. Hirano, and H. Hosono, Appl. Phys. Lett. **77**, 4166 (2000).
[5] H. L. Hartnagel, A. L. Dawar, A. K. Jain, and C. Jagadish, *Semiconducting Transparent Thin Films* (Institute of Physics, Bristol, 1995).
[6] M.R. Lorentz, J.F. Woods, and R.J. Gambino, J. Phys. Chem. Solids **28**, 403 (1967).
[7] T. Harwig, G.J. Wubs, and G.J. Dirksen, Solid State Commun. **18**, 1223 (1976).
[8] R.D. Shannon, J.L. Gillson, and R.J. Bouchard, J. Phys. Chem. Solids **38**, 877 (1977).
[9] F. A. Kröger and H. H. Vink, *Relations Between the Concentrations of Imperfections in Crystalline Solids*, in Solid State Physics Vol. 3, edited by F. Sietz and D. Turnbull (Academic Press Inc., New York, 1956) p. 307.
[10] S. Geller, J. Chem. Phys. **33**, 676 (1960).
[11] Z. Hajnal, J. Miro, G. Kiss, F. Reti, P. Deak, R.C. Herndon, and J.M. Kuperberg, J. Appl. Phys. **86**, 3792 (1999).
[12] E. Aubay and D. Gourier, Phys. Rev. B **47**, 15 023 (1993).
[13] L. Binet and D. Gourier, J. Phys. Chem. Solids **59**, 1241 (1998).
[14] E.G. Víllora, Y. Murakami, T. Sugawara, T. Atou, M. Kikuchi, D. Shindo, and T. Fukuda, Mater. Res. Bull. **37**, 769 (2002).
[15] E.G. Víllora, Y. Morioka, T. Atou, T. Sugawara, and T. Fukuda, Phys. Status Solidi A **193**, 187 (2002).
[16] B. G. Hyde and S. Andersson, *Inorganic Crystal Structures*, (Wiley-Interscience, New York, 1989).
[17] *International Tables for Crystallography*, edited by T. Hahn (Kluwer Academic Publishers, Dordrecht, MA, 1996) Vol. A, p. 158.
[18] E.G. Víllora, M. Yamaga, T. Inoue, S. Yabasi, Y. Masui, T. Sugawara, and T. Fukuda, Jpn. J. Appl. Phys., Part 2 **41**, L622 (2002).
[19] A. Abragam and B. Bleaney, *Electron Paramagnetic Resonance of Transition Ions* (Clarendon Press, Oxford, 1970).
[20] J.H. Van Vleck, Phys. Rev. **74**, 1168 (1948).
[21] G. E. Pake and T. L. Estle, *The Physical Principles of Electron Paramagnetic Resonance* (Benjamin, New York, 1973), p. 170.
[22] O. Madelung, *Introduction to Solid-State Theory* (Springer-Verlag, Berlin, 1978), p. 373.
[23] N. Ueda, H. Hosono, R. Waseda, and H. Kawazoe, Appl. Phys. Lett. **71**, 933 (1997).
[24] L. Binet and D. Gourier, Appl. Phys. Lett. **77**, 1138 (2000).